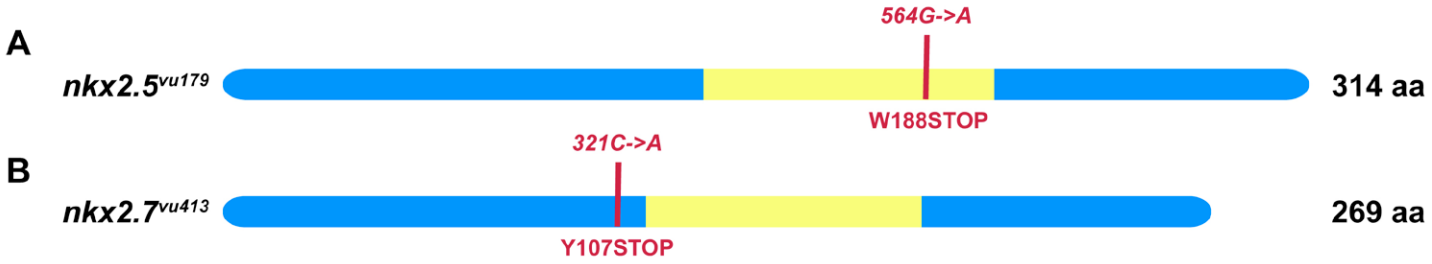

Supplemental Figure S1.

Consequences of TILLING mutations on Nkx2.5 and Nkx2.7 proteins.

Schematics depict the zebrafish Nkx2.5 and Nkx2.7 proteins, with each NK-type homeodomain indicated in yellow. Point mutations generated through TILLING are noted in red with the nucleotide transition/transversion indicated above the protein and the corresponding codon change indicated below. (A) The *nkx2.5*^{vu179} mutation is a G->A transition at position 564 of the open reading frame yielding a nonsense mutation that is predicted to cause truncation of the protein within the homeodomain. (B) The *nkx2.7*^{vu413} mutation is a C->A tranversion at position 321 of the open reading frame leading to a nonsense mutation that is predicted to cause truncation of the protein prior to the homeodomain.

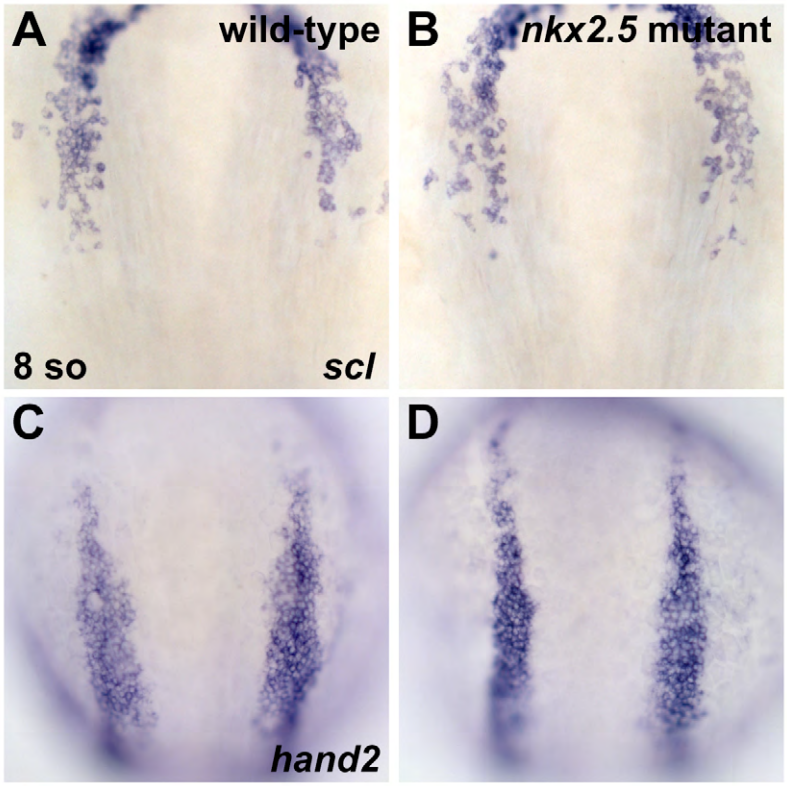

Supplemental Figure S2.

Normal patterning of anterior lateral plate mesoderm in *nkx2.5* mutant embryos.

(**A-D**) In situ hybridization demonstrates expression of *scl* (A,B) and *hand2* (C,D) in wild-type (A,C) and *nkx2.5* mutant (B,D) embryos at the 8 somite stage. Dorsal views, anterior to the top. Gene expression patterns appear normal in *nkx2.5* mutants; no expansion or reduction of heart field size is evident.

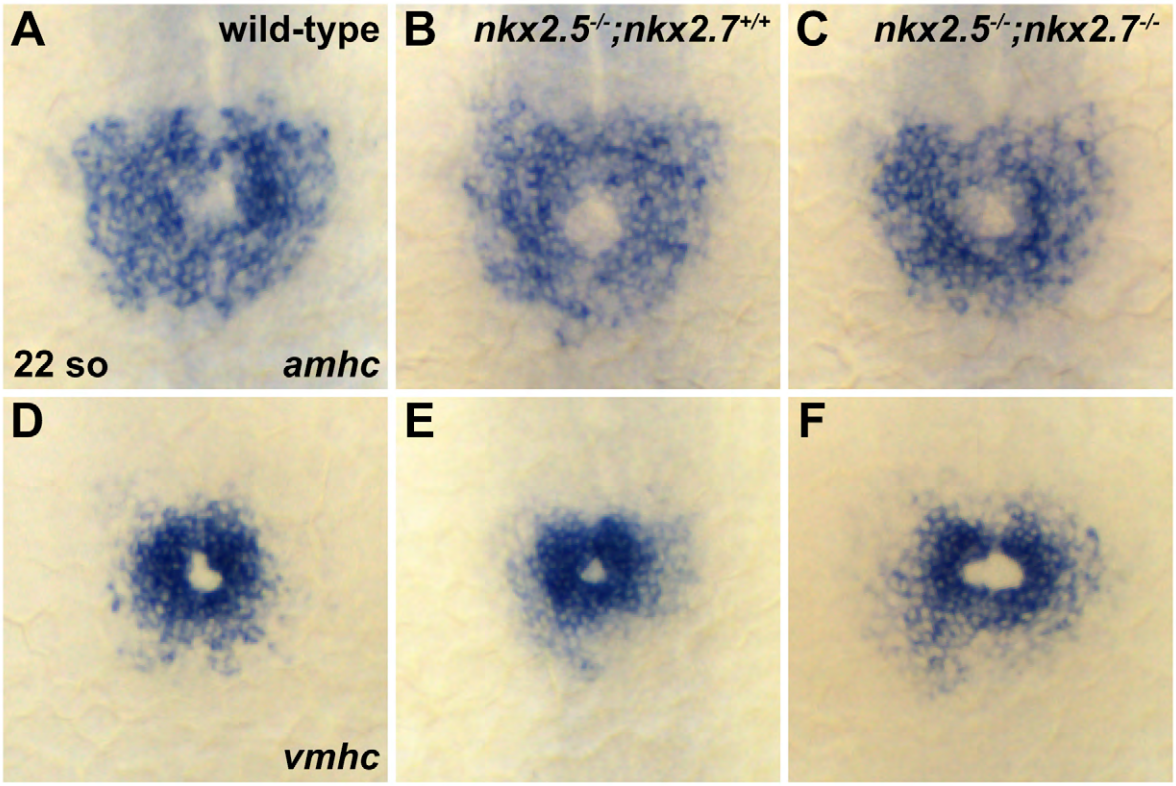

Supplemental Figure S3.

Normal differentiation and fusion of bilateral cardiac precursor populations in *nkx2.5* mutant and *nkx2.5*$^{-/-}$;*nkx2.7*$^{-/-}$ double mutant embryos.

(**A-F**) In situ hybridization depicts expression of *amhc* (A-C) and *vmhc* (D-F) in wild-type (A,D), *nkx2.5* mutant (B,E), and *nkx2.5*$^{-/-}$;*nkx2.7*$^{-/-}$ double mutant (C,F) embryos. Dorsal views, anterior to the top, at the 22 somite stage. Gene expression patterns appear normal in *nkx2.5* mutant and *nkx2.5*$^{-/-}$;*nkx2.7*$^{-/-}$ double mutant embryos; no expansion or reduction of atrial or ventricular precursor populations is evident.

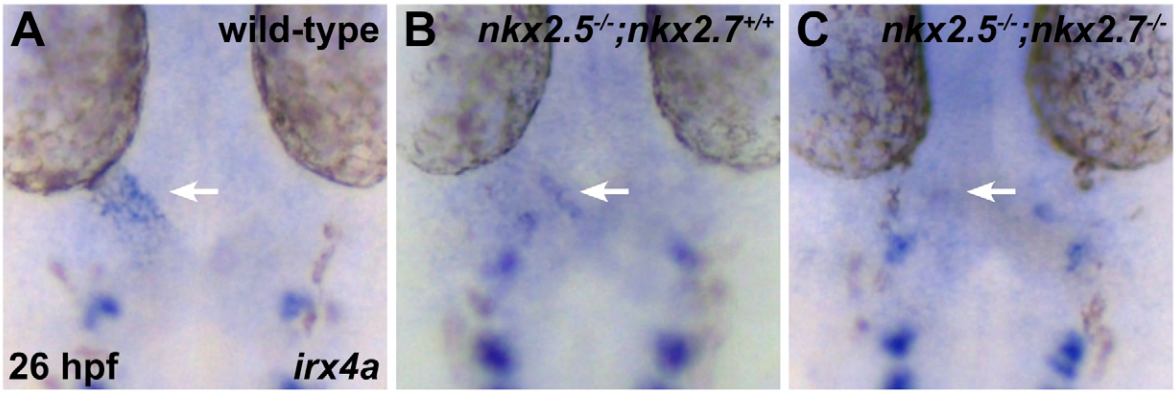

Supplemental Figure S4.

Expression of *irx4a* is progressively downregulated with increased loss of Nkx gene dosage.

(**A-C**) In situ hybridization depicts expression of *irx4a* in wild-type (A), *nkx2.5* mutant (B), and *nkx2.5*$^{-/-}$;*nkx2.7*$^{-/-}$ double mutant (C) embryos. Dorsal views, anterior to the top, at 26 hpf. Ventricular expression of *irx4a* (arrows) is diminished in *nkx2.5* mutants and absent in *nkx2.5*$^{-/-}$;*nkx2.7*$^{-/-}$ double mutants. Expression of *irx4a* is also visible in bilateral neurons of the lateral hindbrain.

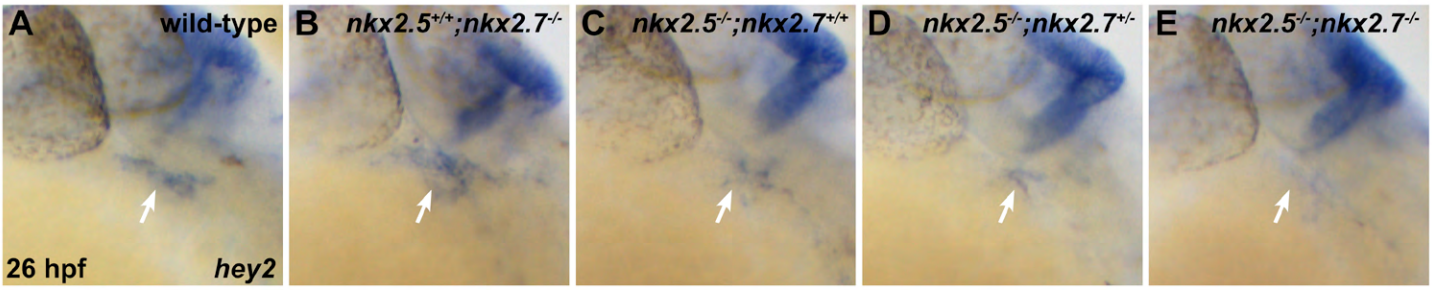

Supplemental Figure S5.

Expression of *hey2* is progressively downregulated with increased loss of Nkx gene dosage.

(**A-E**) In situ hybridization depicts expression of *hey2* at 26 hpf. Lateral views, anterior to the left. *hey2* expression in the ventricle (arrows) is evident in wild-type (A) and *nkx2.7* mutant (B) embryos. However, *hey2* expression is diminished in *nkx2.5* mutant (C) and *nkx2.5*$^{-/-}$;*nkx2.7*$^{+/-}$ mutant (D) embryos and is absent in *nkx2.5*$^{-/-}$;*nkx2.7*$^{-/-}$ mutant embryos (E). Expression of *hey2* is also visible in the diencephalon.

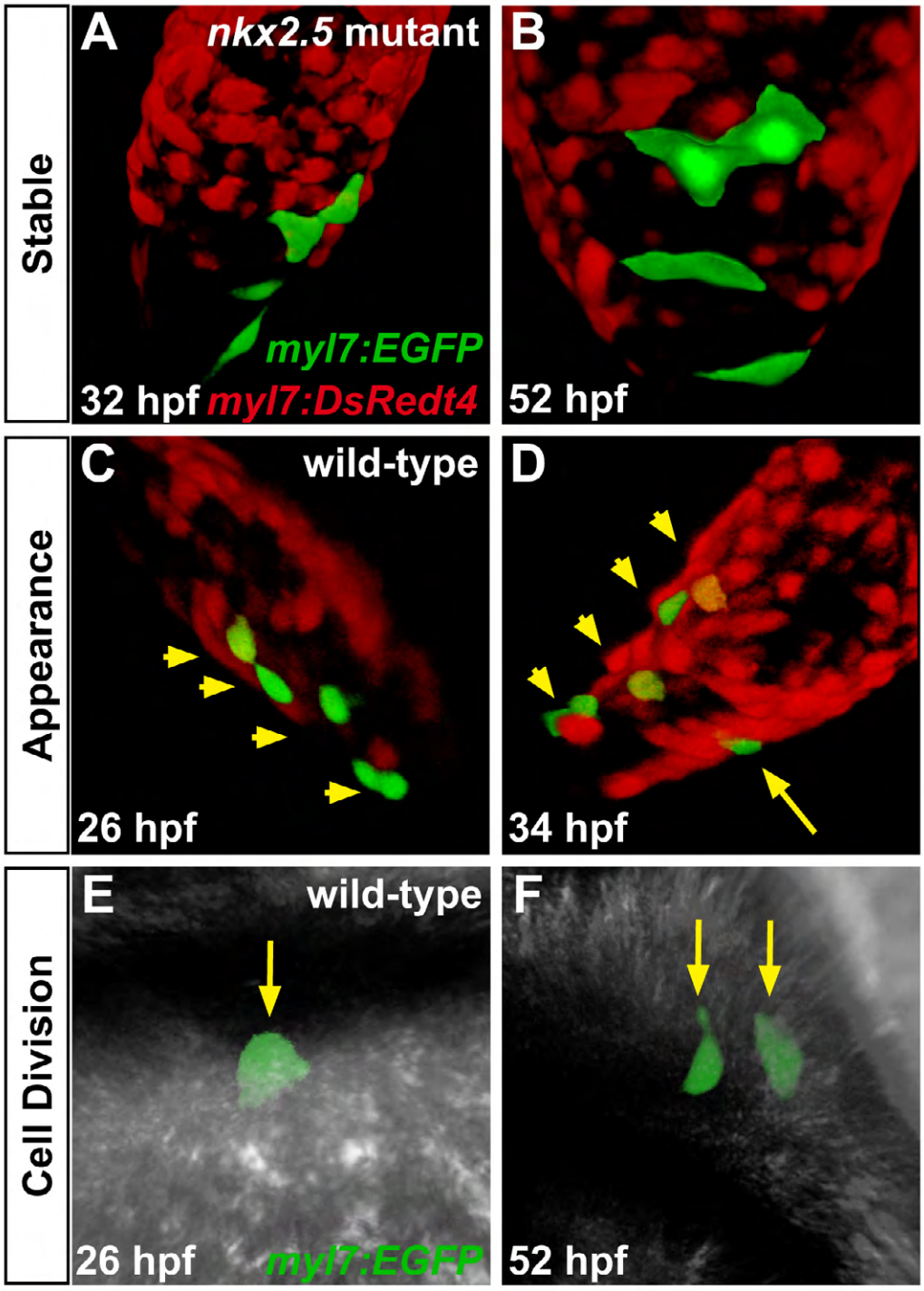
Stable
A
nkx2.5 mutant
myl7:EGFP
32 hpf myl7:DsRedt4
B
52 hpf
Appearance
C
wild-type
26 hpf
D
34 hpf
Cell Division
E
wild-type
26 hpf myl7:EGFP
F
52 hpf

Supplemental Figure S6.

Mosaic labeling tracks cardiomyocyte behavior.

Confocal projections of mosaic hearts in live zebrafish embryos. Mosaic labeling was performed by injecting *Tg(myl7:EGFP)* plasmid into *nkx2.5* mutant embryos and their wild-type siblings, both of which carried *Tg(myl7:DsRedt4)*. Embryos with 2-6 GFP-positive cells were followed from 26 to 52 hpf, allowing for detailed analysis of cell behaviors, including division, appearance, and disappearance of cardiomyocytes.

(**A-F**) Representative examples of observed cell behavior scenarios. The observed frequency of occurrence of each scenario in wild-type and *nkx2.5* mutant embryos is provided in Table S1. (A,B) Most cells remained stable during the tracking period; as shown in this example, 4 GFP-positive cells in the atrium of a *nkx2.5* mutant heart exhibit stable morphology and orientation. (C,D) In some embryos, new GFP-positive cells appeared during the tracking period; in this example, a new GFP-positive cell (yellow arrow in D) appears in a wild-type atrium. Given the distance between the new GFP-positive cardiomyocyte and the 4 originally labeled cells (yellow arrowheads in C and D), the new cell is not likely to be the product of cell division. Instead, newly appearing cells most likely reflect delayed initiation of *myl7* expression in late-differentiating, SHF-derived cardiomyocytes (de Pater et al., 2009; Hami et al., 2011; Lazic and Scott, 2011; Zhou et al., 2011). (E,F) Cell division was occasionally observed; in this example, a single cardiomyocyte (yellow arrow in E) in a wild-type embryo gives rise to two daughter cells (yellow arrows in F).

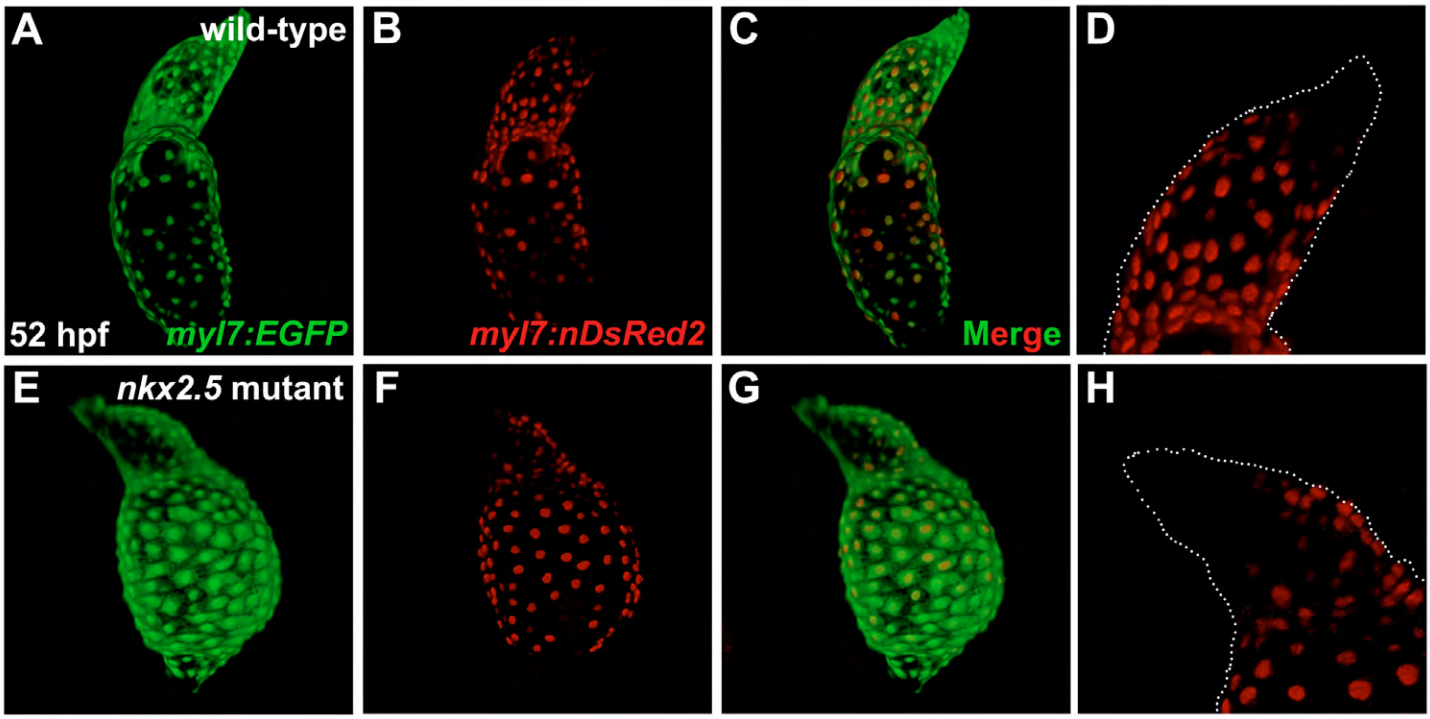

Supplemental Figure S7.

Developmental timing assay indicates late-differentiating cells added to the arterial pole of the *nkx2.5* mutant heart.

Confocal projections of hearts in live wild-type (A-D) and *nkx2.5* mutant (E-H) embryos expressing *Tg(myl7:EGFP)* (A,E) and *Tg(-5.1myl7:nDsRed2)* (B,D,F,H). Lateral views, arterial pole to the top, at 52 hpf. (D,H) White dots outline the morphology of the *Tg(myl7:EGFP)*-expressing ventricle and outflow tract.

(**A-D**) In the wild-type heart, the late-differentiating cardiomyocyte population exhibits green, but not red, fluorescence, due to the delay in expression of *Tg(-5.1myl7:nDsRed2)*, in comparison with expression of *Tg(myl7:EGFP)*, at the arterial pole (de Pater et al., 2009).

(**F-H**) Similarly, in the *nkx2.5* mutant heart, cardiomyocytes expressing *Tg(myl7:EGFP)*, but not *Tg(-5.1myl7:nDsRed2),* are present at the arterial pole.

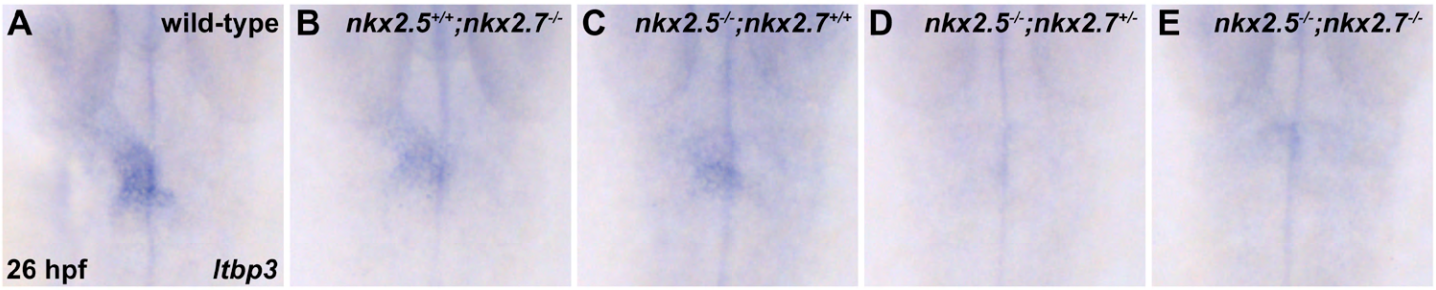

Supplemental Figure S8.

Expression of *ltbp3* is downregulated in *nkx2.5* mutant and *nkx2.5*$^{-/-}$;*nkx2.7*$^{-/-}$ double mutant embryos.

(**A-E**) In situ hybridization depicts expression of *ltbp3* at 26 hpf. Dorsal views, anterior to the top. *ltbp3* expression is visible at the arterial pole in wild-type (A) and *nkx2.7* mutant (B) embryos. However, *ltbp3* expression is reduced in *nkx2.5* mutant embryos (C) and is absent in *nkx2.5*$^{-/-}$;*nkx2.7*$^{+/-}$ (D) and *nkx2.5*$^{-/-}$;*nkx2.7*$^{-/-}$ (E) mutant embryos.

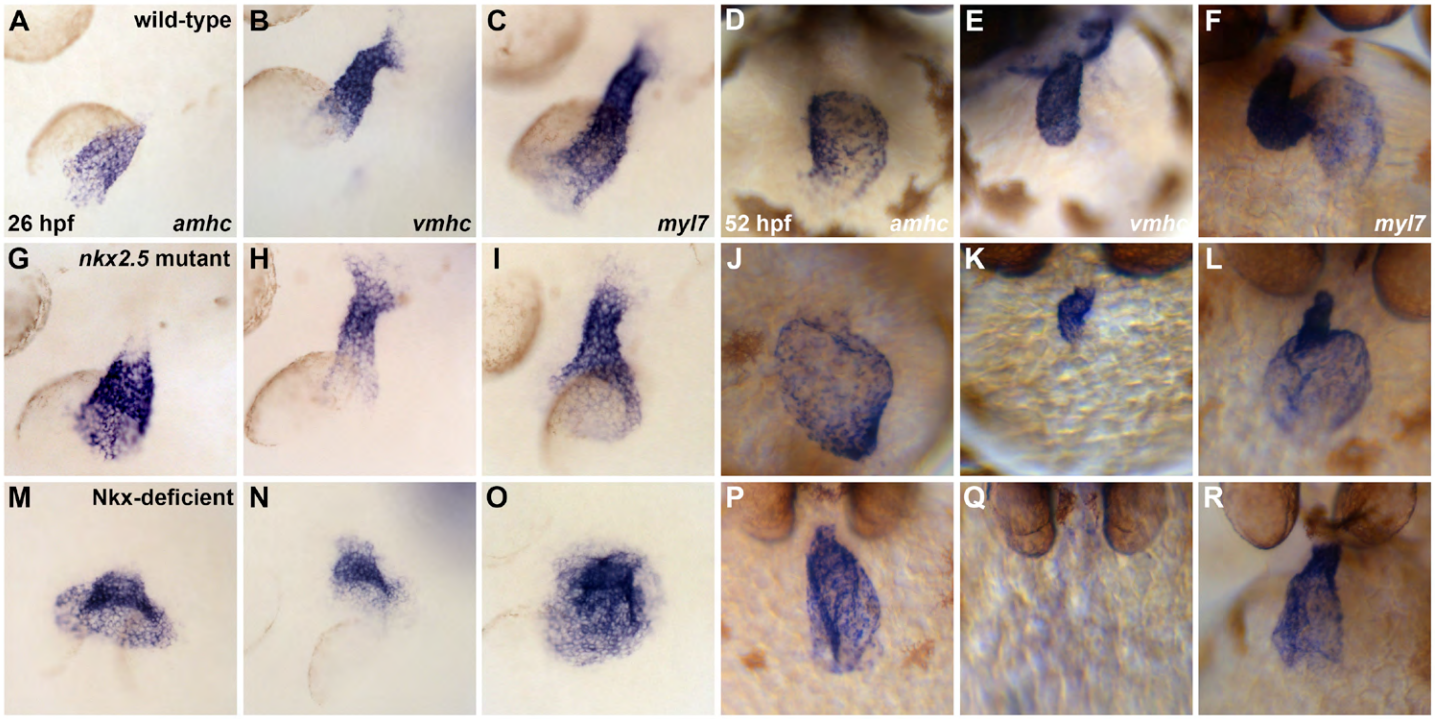

Supplemental Figure S9.

Gene expression patterns indicate ventricular and atrial territories.

In situ hybridization illustrates expression patterns of *amhc* (A,D,G,J,M,P), *vmhc* (B,E,H,K,N,Q), and *myl7* (C,F,I,L,O,R) at 26 (A-C,G-I,M-O) and 52 hpf (D-F,J-L,P-R). Representative examples of wild-type (A-F), *nkx2.5* mutant (G-L) and Nkx-deficient (M-R) embryos clarify the territories generally considered to be expressing *vmhc* or *amhc* when conducting and interpreting photoconversion experiments (Fig. 9).

Supplemental Table S1.

Mosaic labeling does not detect significant changes in cardiomyocyte behavior in *nkx2.5* mutants.

	Number of Observed Occurrences			
	Cell Division	Cell Appearance	Cell Loss	Total Embryos
wild-type	6	18	5	42
	14%	43%	12%	
nkx2.5 mutant	4	7	1	13
	31%	54%	8%	

Mosaic labeling experiments (as described in Fig. S6) were conducted in *nkx2.5* mutant embryos (n=13) and their wild-type siblings (n=42). The number of observed occurrences of each cell behavior (cell division, cell appearance, or cell loss) is indicated. No significant differences in the frequencies of these events were observed in our comparisons between wild-type and *nkx2.5* mutant embryos. Although cell division was seen more frequently in *nkx2.5* mutant embryos, these events were not exclusively seen in the atrium and are therefore not likely to account for the excess atrial cardiomyocytes in *nkx2.5* mutant embryos. Overall, most tracked cells remained stable between 26 and 52 hpf, rather than disappearing or dividing.